

# Bioinspiration & Biomimetics



## PAPER

# Hydrodynamic advantages of in-line schooling

Mehdi Saadat<sup>1,2,\*</sup>, Florian Berlinger<sup>3</sup>, Artan Sheshmani<sup>4,5,6</sup>, Radhika Nagpal<sup>3</sup>, George V Lauder<sup>1</sup> and Hossein Haj-Hariri<sup>2</sup>

<sup>1</sup> Department of Organismal and Evolutionary Biology, Harvard University, Cambridge, Massachusetts 02138, United States of America

<sup>2</sup> Department of Mechanical Engineering, University of South Carolina, Columbia, South Carolina 29208, United States of America

<sup>3</sup> School of Engineering and Applied Sciences, Harvard University, Cambridge, Massachusetts 02138, United States of America

<sup>4</sup> Center for Mathematical Sciences and Applications, Harvard University, Department of Mathematics, Cambridge, MA, 02139, United States of America

<sup>5</sup> Department of Mathematics, Aarhus University, Ny Munkegade 118, building 1530, 319, 8000 Aarhus C, Denmark

<sup>6</sup> National Research University Higher School of Economics, Russian Federation, Laboratory of Mirror Symmetry, NRU HSE, 6 Usacheva str., Moscow, Russia, 119048

\* Author to whom any correspondence should be addressed.

E-mail: [msaadat@fas.harvard.edu](mailto:msaadat@fas.harvard.edu)

**Keywords:** schooling, fish swimming, bioinspired robots, hydrodynamic interaction, energy harvesting, collective motion

Supplementary material for this article is available [online](#)

## Abstract

Fish benefit energetically when swimming in groups, which is reflected in lower tail-beat frequencies for maintaining a given speed. Recent studies further show that fish save the most energy when swimming behind their neighbor such that both the leader and the follower benefit. However, the mechanisms underlying such hydrodynamic advantages have thus far not been established conclusively. The long-standing drafting hypothesis—reduction of drag forces by judicious positioning in regions of reduced oncoming flow—fails to explain advantages of in-line schooling described in this work. We present an alternate hypothesis for the hydrodynamic benefits of in-line swimming based on enhancement of propulsive thrust. Specifically, we show that an idealized school consisting of in-line pitching foils gains hydrodynamic benefits via two mechanisms that are rooted in the undulatory jet leaving the leading foil and impinging on the trailing foil: (i) leading-edge suction on the trailer foil, and (ii) added-mass push on the leader foil. Our results demonstrate that the savings in power can reach as high as 70% for a school swimming in a compact arrangement. Informed by these findings, we designed a modification of the tail propulsor that yielded power savings of up to 56% in a self-propelled autonomous swimming robot. Our findings provide insights into hydrodynamic advantages of fish schooling, and also enable bioinspired designs for significantly more efficient propulsion systems that can harvest some of their energy left in the flow.

## 1. Introduction

Many explanations have been provided for the schooling behavior of fishes [1, 2]. Of specific interest has been the question of whether the fluid-mediated interactions of schooling impart energy savings to the group, or to the individual [3, 4]. Recent advances have shown that fish do in fact save on the cost of movement when swimming in groups, and their energy savings are maximized when swimming behind their neighbor [5]. In such tandem arrangement, even the leading fish appear to save on the cost of movement. But conclusive hydrodynamic mechanisms underlying such energy savings have not

been identified yet. A prevalent hypothesis predicts fish can save energy by judiciously placing themselves in the regions of the school with reduced oncoming flow in the vortical wake left by the leading fish [3]. A diamond pattern then arises as a natural consequence of such drag-reduction mechanism. But there has been increasing evidence against such diamond formation in biological observations [5–8]. In particular, the drag-reduction hypothesis fails to explain the energy benefits seen in schools of fish [5] and models of self-propelled in-line swimming [9–14] where one swimmer is directly inside the thrust wake of another swimmer and encounters higher flow speed than surroundings. Therefore, it remains unknown how

fish might benefit energetically when swimming in tandem.

In this work, we propose an alternative hypothesis based on the enhancement of propulsive thrust. Specifically, fish interacting with the undulatory thrust-wake leaving an upstream fish in a school may benefit from suction on their snout, while in turn providing a favorable push on that same upstream fish by enhancing the hydrodynamic added-mass experienced by its tail. We provide evidence to support this hypothesis through computational analyses, mathematical modeling, and experiments using a purpose-built robotic platform.

Pitching foils (and flapping foils in general) have been used extensively as surrogates for fish to gain insight into their unsteady locomotion [11, 15–18]. A notable recent series of studies have investigated the dynamics of an array of heaving foils cruising in tandem as an idealized model of a school [11, 14, 19]. Even though this approach has led to uncovering many interesting dynamical features of schooling, including hysteresis in the swimming speed-flapping frequency response, these studies are either constrained to a fixed intra-school distance [19], or do not report hydrodynamic power consumption [11, 14] which is critical to assessing hydrodynamic efficiency of the group. Such shortcomings have made it difficult to identify the hydrodynamic mechanisms leading to saving energy in schooling, specifically at small intra-school distances. We address these shortcomings by allowing the intra-school distance and Reynolds number to be independent variables so that the full parameter space is investigated.

## 2. Materials and methods

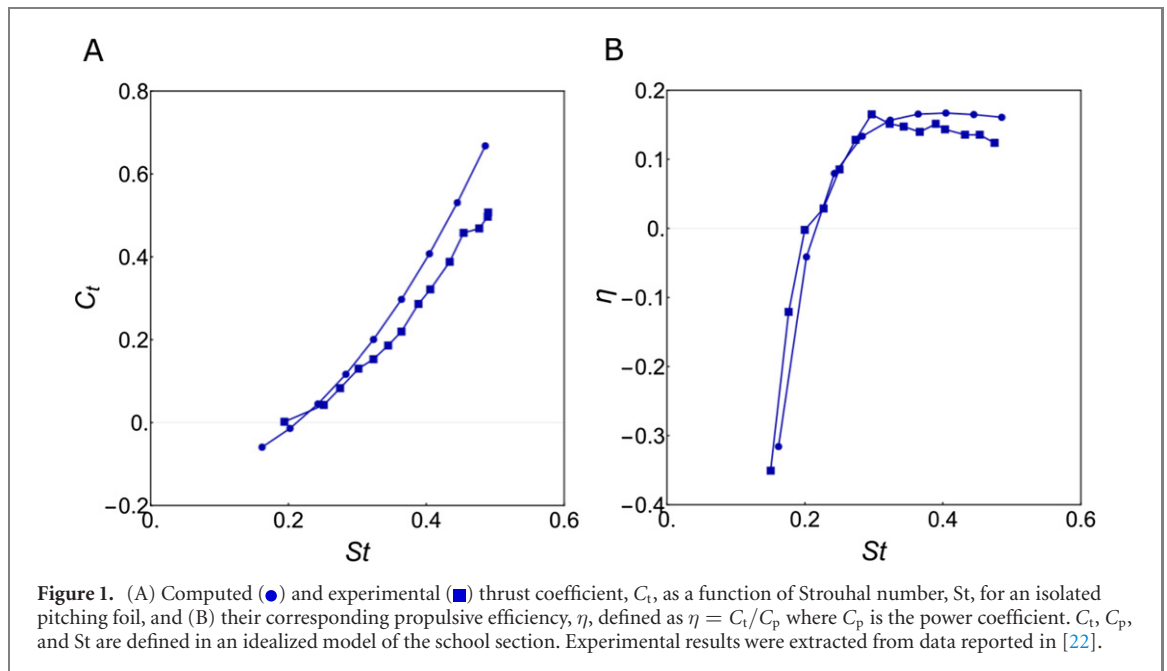
**Simulations.** We use commercial computational fluid dynamics (CFD) package ANSYS® CFX, release 18.0 to discretize and solve two-dimensional unsteady incompressible Reynolds-averaged Navier–Stokes equations based on a hybrid finite-volume/finite-element approach [20]. We further choose the shear stress transport turbulence model [21] to calculate the Reynolds Stress terms due to its good capability to predict the onset and amount of flow separation under adverse pressure gradient conditions while also handling the laminar to turbulent transition.

Foils with NACA0012 cross section and chord length  $c = 0.068$  (m) placed in rectangular domains are used for all cases except when stated otherwise. Horizontal periodic conditions are imposed on the inlet and outlet boundaries for the infinite school. To achieve horizontal periodicity, a mass flow rate based on the given free-stream Reynolds number is specified across the inlet–outlet boundary conditions. The solver implements the specified mass flow rate by modifying the pressure change across the inlet–outlet boundary conditions until it is satisfied. The average flow speed on the boundaries is then that of the

swimming speed for the school. For the rest of the cases with finite number of foils, velocity/atmospheric pressure are imposed on the inlet/outlet boundaries extended  $40c$  away from the foils. The domain is bounded vertically by shear-free walls extended  $40c$  for all cases. An unstructured grid is used in the simulations with a total number of approximately 300 000 elements and the minimum grid spacing of  $0.000125c$ . The mesh is finest around each foil and gradually coarsens away with the same resolution for all cases. The maximum non-dimensional normal distance of the first node above the surface of the foil is  $y^+ = u^*y/\nu \approx 0.35$  when the foil is at its maximum flapping speed, where  $u^*$ ,  $y$ , and  $\nu$  are the nearest-wall friction velocity, normal distance away from the wall, and kinematic viscosity, respectively.

The oscillatory motion of the pitching foils is described with  $(A/2c)\sin(2\pi ft)$  where  $A$  is the trailing edge tip-to-tip amplitude. The time step is chosen such that the solver uses 500 steps in each flapping period for all cases. The time-averaged net force is computed after the dissipation of the startup transients for each simulation and is zero in normal direction by symmetry for all cases given that the frequency and amplitude of flapping is small. To find the emergent dynamics in self-propelled cases, we first prescribe a given intra-school distance and swimming speed and then we search for the frequency at which the time-averaged net forward force acting on the foil is zero. Instantaneous hydrodynamic power deposited into the flow is calculated as the torque around the leading edge multiplied by the angular velocity of the foil.

To better showcase the accuracy of the solver, we have conducted a set of simulations for an isolated pitching foil and compared the calculated forces and power with experiments reported in [22]. The foil has a teardrop cross-section, and its dimensions were adopted exactly as is reported in [22], with a chord length of  $c = 80$  mm and maximum thickness of 8 mm. The oncoming flow speed is kept at  $60 \text{ mm s}^{-1}$  which results in a chord-based Reynolds number of  $\text{Re} = 5400$ . The maximum pitching angle is further kept constant at  $\theta = 7^\circ$ .  $\text{Re}$  and  $\text{St}$  are defined in the an idealized model of the school section. Figures 1(A) and (B) shows calculated time-averaged forward thrust and propulsive efficiency as a function of Strouhal number and compares the values with experimental counterparts. Thrust is calculated by subtracting drag from net forward force on the foil. The comparison exhibits that the numerical modeling provides excellent prediction of forces and power on the pitching foil for the relevant range of Strouhal number considered here,  $\text{St} < 0.25$ . Finally, to ensure the solution is mesh independent, we have chosen the case with  $\text{St} = 0.24$  and conducted two more simulations with mesh resolutions of approximately 75% and 50% of the original mesh. The calculated time-averaged thrust and power had less than



2.5% variance among all three cases, confirming the mesh independency of the final solution.

**Robotic Design and Experiments.** We use the experimental Finbot platform [23–25] to investigate the performance of a novel propulsor consisting of a stationary foil positioned in-line behind the caudal fin and attached to the main body using a ring. The attached foil and ring are rigid and 3D-printed on a Stratasys PolyJet Objet500 in Verowhite material. The caudal fin is soft and laser-cut from flexible plastic shims (Artus Corp). Finbot has a 122 mm long streamlined body attached to a 22 mm long caudal fin, inspired in shape by the blue tang (*Paracanthurus hepatus*). It is carefully designed to mimic fish swimming (see discussions in [24]). Finbot has four individually controllable fins for autonomous underwater swimming. It uses sensory feedback from an inertial (InvenSense MPU-9250) and pressure sensor (TE connectivity MS5803-02BA) for heading and depth control, respectively. Notably, Finbot has onboard power monitoring and logging (Texas Instruments INA219) as described in our previous work [24, 25].

A typical experiment is executed as follows: First, we initialize Finbot at the water surface of one end of a tank (66 cm  $\times$  28 cm  $\times$  28 cm) such that it is aligned with the target swimming direction; second, we carefully release the Finbot at the programmed target depth of 10 cm below the surface; third, Finbot swims toward the other end of the tank, maintaining a straight-line course and constant diving depth. We repeat such experiment for five frequencies from 0.75 Hz to 1.75 Hz, and combined  $N = 5$  trials per data point to report the mean  $\mu$  and standard deviation  $\sigma$ .

We measure cruise speed and power for three cases, namely (i) the robot only, (ii) the robot with the foil positioned closely behind the tip of the caudal

fin (with a separation distance  $d < 1$  mm), and (iii) the foil positioned far from the tip of the caudal fin ( $d \sim 22$  mm). The foil has NACA0020 cross section that spans 75 mm by 48 mm in span and chord direction and is fabricated to be neutrally buoyant such that it does not affect the balance of the robot. The flapping amplitude of the caudal fin is held constant throughout the experiments at 20% of the total length of Finbot (from head to the tip of the caudal fin) since this ratio is found to minimize the energy expenditure of swimming experimental fish surrogates [26]. Across all frequencies, we impose sinusoidal actuation signals for oscillatory caudal fin motions, i.e. for smooth changes of direction at peak amplitude.

The input voltage available to the caudal actuator at any given frequency is selected to be identical for all cases. Consequently, power consumption across all cases with the same flapping frequency has statistically insignificant variations and can be considered equal. However, the resulting cruise speeds are different, with the robot and close foil [case (ii)] outperforming the robot only [case (i)] and the robot and far foil [case (iii)], supporting our theory and simulations. Case (iii) is chosen as a control case to isolate the performance improvements and attribute them to the hydrodynamic, i.e. to the leading edge suction on the foil and the added mass push on the caudal fin, as opposed to, for instance, a reduction in head oscillations.

For the analysis of swimming speeds, we record videos with a Photron Mini-UX100 high-speed camera at 250 frames per second and a resolution of 1280  $\times$  1024 pixels. To achieve a high degree of repeatability and standardization in the way we analyze the video data, we train a state-of-the-art deep convolutional neural network-based tracking code

[27] to identify Finbot and output its pixel coordinates in each frame, from which we calculate cruise speed. Power consumption for forward propulsion is measured with an onboard power monitor at a sampling rate of approximately 30 Hz, and averaged over the course of an experiment to a single mean power.

### 3. Results and discussion

#### 3.1. An idealized model of the school

To start, we devise an idealized model of the school consisting of an infinite array of self-propelled two-dimensional pitching foils arranged in tandem configuration (figure 2(A)). This elementary model allows for the systematic study of the hydrodynamics of schooling when each foil swims in the thrust-wake left by another foil.

Several dimensionless parameters characterize the schooling problem. Cruise speed of the school,  $U$ , is a function of flapping frequency,  $f$ , flapping amplitude,  $A$ , intra-school distance,  $D$ , swimmer length,  $c$ , and fluid density,  $\rho$ . Shape and surface properties of the swimmer are captured in drag coefficient,  $C_d$  ( $= 2\bar{D}/(\rho c U^2)$ ), while the thrust characteristics are captured in thrust coefficient,  $C_T$  ( $= 2\bar{T}/(\rho c U^2)$ ). Drag,  $\bar{D}$ , and thrust,  $\bar{T}$ , are defined as the time-averaged forces on each swimmer in downstream and upstream directions, respectively. In cruise, there is no acceleration, so that  $\bar{T}$  is equal to  $\bar{D}$ , and  $C_T$  is equal to  $C_d$ .

The dimensional functional relationship (denoted as  $F$ ) for the cruise speed of the school (same for an individual swimmer [26]) can be described as:

$$U = F(f, A, c, D, C_d). \quad (1)$$

We note that  $C_d$  is a function of Reynolds number,  $Re(= Uc/\nu)$  where  $\nu$  ( $= \mu/\rho$ ) is the kinematic viscosity, and  $\mu$  denotes the viscosity of the fluid. A dimensionless form of the equation (1) is then:

$$\frac{fc}{U} = \phi\left(\frac{A}{c}, \frac{D}{c}, Re\right). \quad (2)$$

Equation (2) couples  $f^*(= fc/U)$ ,  $A^*(= A/c)$ ,  $D^*(= D/c)$ , and  $Re$ , and therefore describes all possible cruise states for the school.  $A^*$  is held fixed throughout the study with a value ( $= 0.2$ ) corresponding to efficient locomotion of fish in isolation [26, 28, 29] and in school [30]. Strouhal number,  $St = f^* A^*$ , an important parameter describing fish locomotion, is then directly related to  $f^*$ , also known as reduced frequency.  $f^*$  and  $D^*$  are physically meaningful:  $f^*$  is inversely related to the dimensionless wavenumber of the wave-like flow left behind by each foil (figure 2(B)), and  $D^*$  corresponds to the intra-school distance. The form of the function  $\phi$  is determined both computationally, and from theory, in the following sections.

#### 3.2. Simulation of the school

To gain insight into the emergent dynamics of the idealized model of a school at cruise (figure 2), we conduct CFD simulations on a single pitching foil that is swimming freely in its own wake in a repeating cell created by imposing periodic boundary conditions on the inlet and outlet boundaries (see methods). This model therefore simulates an infinite school of in-phase pitching foils arranged in tandem configuration with identical kinematics. The goal is to calculate all triplets ( $f^*$ ,  $D^*$ ,  $Re$ ) that result in zero net forward force on the foil (i.e. cruise condition), and to obtain the input hydrodynamic power coefficient,  $C_p = 2\bar{P}/(\rho c U^3)$ , where  $\bar{P}$  denotes the hydrodynamic power deposited by the foil into the fluid.

Simulations indicate that the school benefits energetically from the intra-school interactions for nearly all the cases studied here. As is shown in figures 3(A)–(D), nearly for every combination of  $Re$  and  $D^*$ , we see lower values for  $f^*$  and  $C_p$  in the one-dimensional school compared to an isolated cruising pitching foil. A lower value for  $f^*$  and  $C_p$  implies more efficient swimming, as the swimmer does not need to flap as rapidly to cruise at a desired speed. To better understand the mechanisms underlying such energy savings, we recall that the periodic shedding of vortices left by the trailing edge of the immediate leader causes the fluid jet to not point straight rearward (as one might surmise based on a time-averaged view of the world), but be undulatory (figures 3(E) and (F)). These vortices are a signature of fish locomotion [31]. The interaction of the wave-like jet with the immediate follower produces two effects, (i) the follower experiences an oscillating effective angle of attack in the vicinity of its leading edge. This oscillating angle of attack causes the (circulatory) lift force that is instantaneously normal to the oscillating direction of the oncoming flow, and which always has a component in the forward direction which appears as streamwise suction around the leading edge. This phenomenon was first described by Knoller and Betz in the early 1900s [32], and (ii) blockage of the unsteady jet by the follower's leading edge increases the effective added mass forces on the leader's trailing edge manifested by an increase in pressure, which then, reactively (and instantaneously), increases the thrust on the leader and effectively pushes the leader forward (see movie S1 (<http://stacks.iop.org/BB/16/046002/mmedia>)). Comparison of the time-averaged pressure over the surface for the isolated swimmer with that of the school at two different intra-school distances (figure 4) shows the presence of both suction around the leading edge and high pressure on the aft portion of the foil as the result of the interaction. These effects are significantly enhanced as the intra-school distance is shortened.

For short intra-school distances, a pitching foil inside the infinite school benefits from both the leading-edge suction and the enhanced added-mass



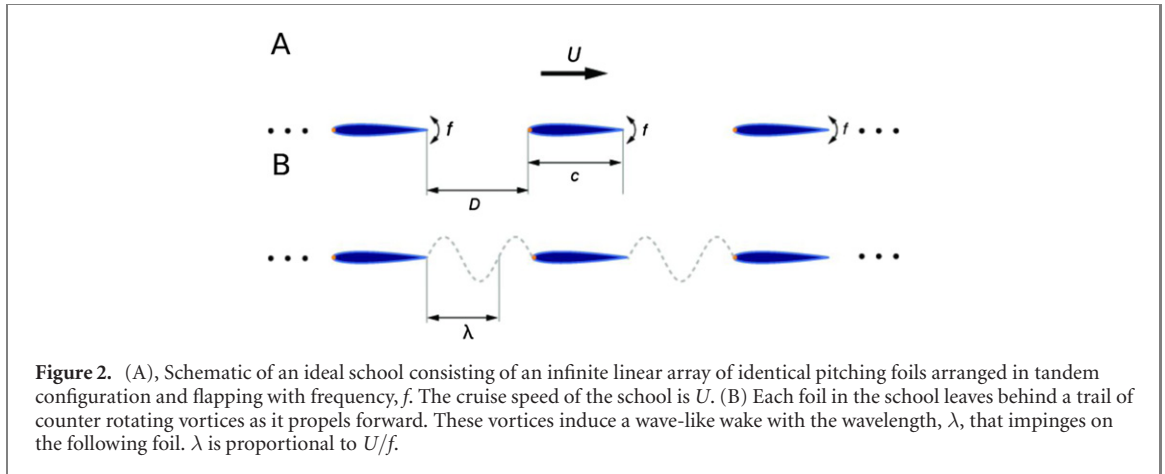


**Figure 2.** (A), Schematic of an ideal school consisting of an infinite linear array of identical pitching foils arranged in tandem configuration and flapping with frequency,  $f$ . The cruise speed of the school is  $U$ . (B) Each foil in the school leaves behind a trail of counter rotating vortices as it propels forward. These vortices induce a wave-like wake with the wavelength,  $\lambda$ , that impinges on the following foil.  $\lambda$  is proportional to  $U/f$ .

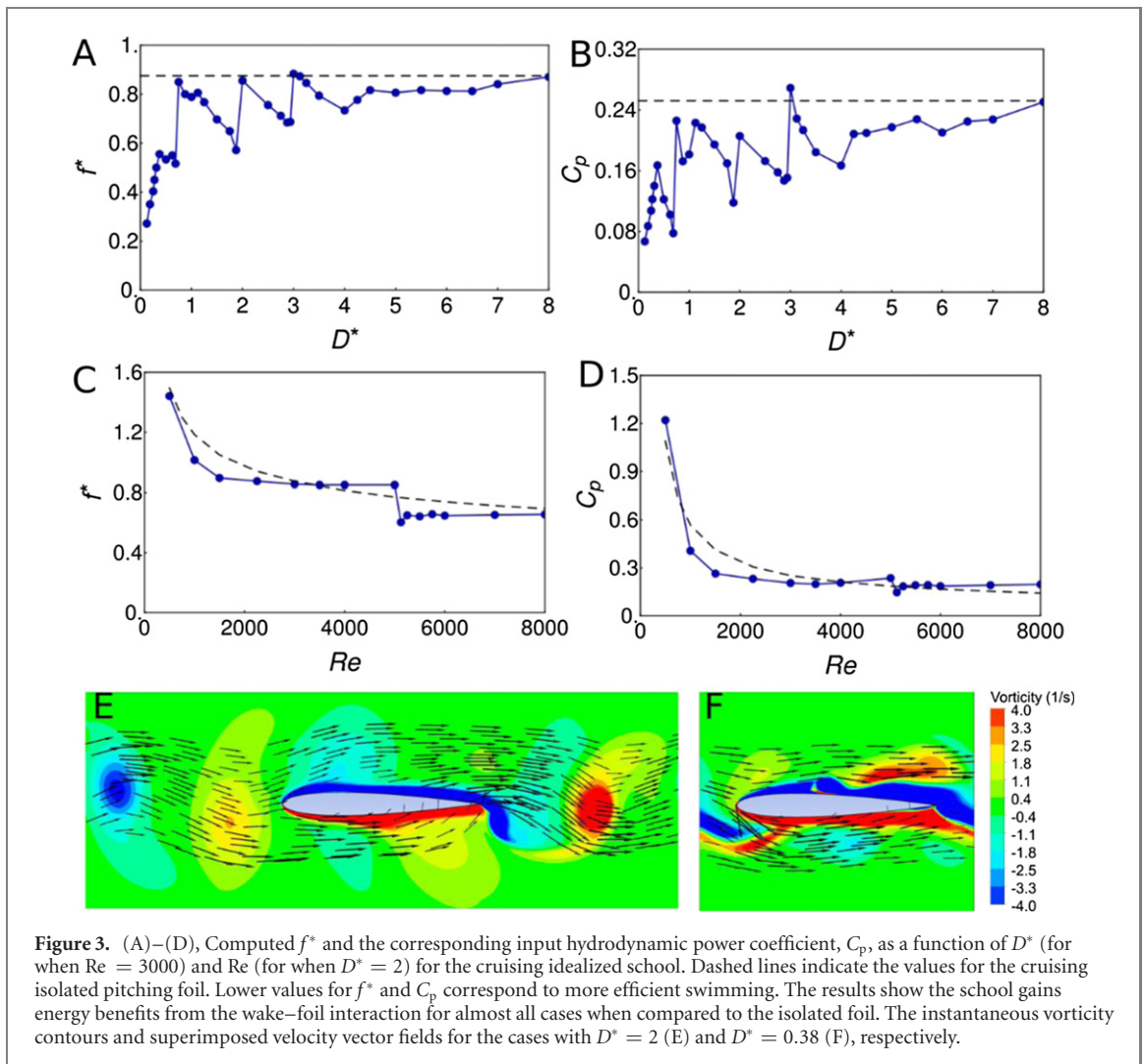
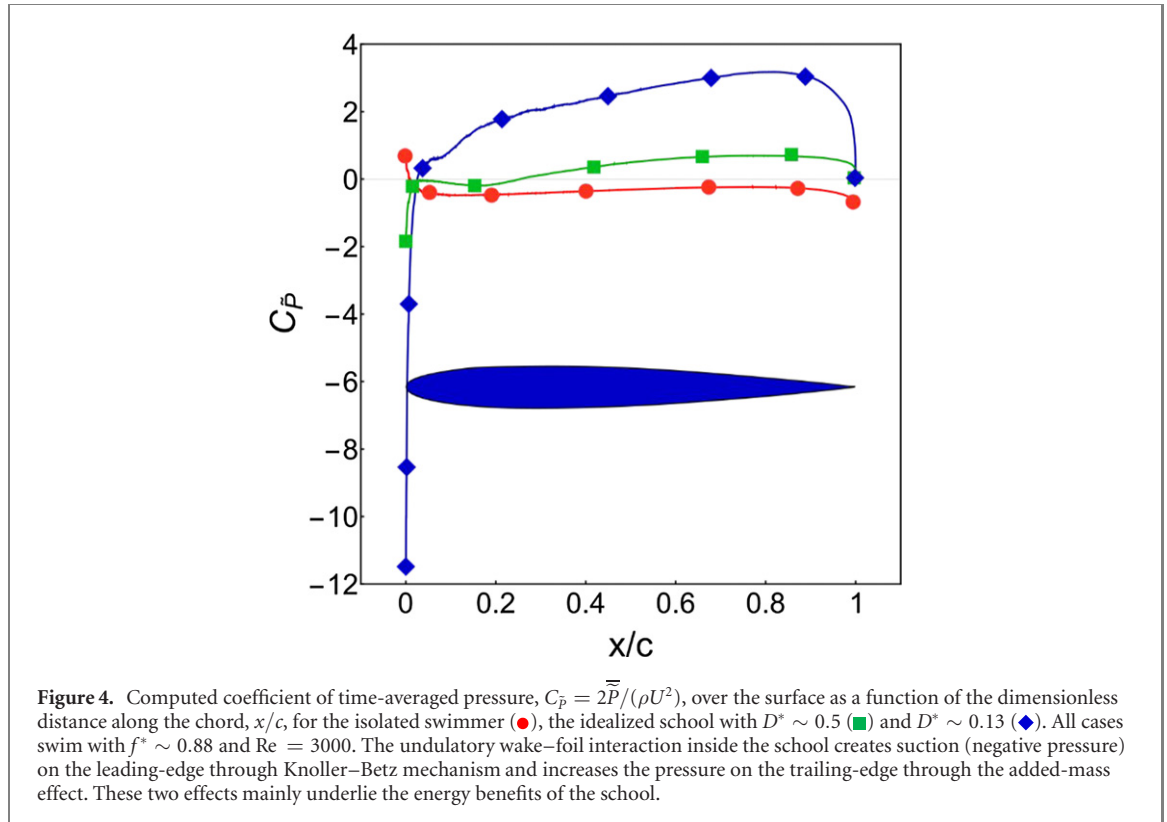


**Figure 3.** (A)–(D), Computed  $f^*$  and the corresponding input hydrodynamic power coefficient,  $C_p$ , as a function of  $D^*$  (for when  $Re = 3000$ ) and  $Re$  (for when  $D^* = 2$ ) for the cruising idealized school. Dashed lines indicate the values for the cruising isolated pitching foil. Lower values for  $f^*$  and  $C_p$  correspond to more efficient swimming. The results show the school gains energy benefits from the wake–foil interaction for almost all cases when compared to the isolated foil. The instantaneous vorticity contours and superimposed velocity vector fields for the cases with  $D^* = 2$  (E) and  $D^* = 0.38$  (F), respectively.

effects, and the energy benefits are maximized with greater than 70% improvement in  $f^*$  and  $C_p$  at the shortest  $D^*$ . The hydrodynamic interactions inside a school serve as extra sources of thrust on the foil, compared with the thrust of an isolated pitching foil which is generated by means of accelerating a volume of the fluid downstream using mainly its trailing edge. In other words, interaction of a pitching foil with the replica of its own wavy flow (from the identical foil

in the repeating cell ahead) remains essentially always constructive, which explains the general decrease in  $f^*$  and  $C_p$  in a school for essentially all  $D^*$ . This is a feature of the pitching motion (which better represents a swimming fish [26]), and is distinctly *not* observed in heaving foils [10, 19]. This is because the thrust of an isolated heaving foil is mainly generated by the leading-edge suction and therefore a destructive interaction with the oncoming undulatory flow leads to



a near complete-loss of thrust when swimming in a group in tandem.

The simulations feature distinctive jumps in the values of  $f^*$  and corresponding  $C_p$  for several values of intra-school distances in the range  $0.75 \lesssim D^* \lesssim 4.5$ . When viewed dimensionally (figure S1), the results show that speed (and corresponding power) experiences a hysteresis phenomenon in that the abrupt increase in  $U$  (and  $P$ ) for *increasing*  $f$  is not equal to the change in  $U$  (and  $P$ ) when *decreasing*  $f$ . The jumps (and hysteresis) in the emergent dynamics of the school are represented as folds of the cruise solution-surface of the school in the three-dimensional ( $f^*$ ,  $D^*$ ,  $Re$ ) parameter space. More specifically, and as will be shown by a mathematical model next, the folds are the outcome of the interference of the undulatory wake left by a leader with the periodic motion of its immediate follower. Similar jumps in the swimming speed vs flapping frequency were observed for an infinite one-dimensional school of heaving foils having a fixed intra-school distance [19], and later shown for two heaving foils with variable distance [14] and frequency [11]. We note that these abrupt changes are energetically detrimental (e.g. when the school starts from rest) as the abrupt gain in speed is intertwined with an even larger relative jump in the hydrodynamic input power, resulting in an increase in the cost of transport [defined here as  $P/U$ , figure S1(B)]. Our results further show that when the intra-school distance is short ( $D^* \lesssim 0.75$ ), the jumps in the solution effectively disappear, and energy efficiency of the school is maximized.

### 3.3. A mathematical model of the one-dimensional school

Building on the insights from the computational results, we provide a mathematical model that captures the dominant features of the emergent dynamics of the idealized school. We build on the general format adopted by [11, 19] to describe the dynamics of a school of swimming foils. We address several of the limitations of existing models by retaining the intra-school distance and Reynolds number as independent variables to provide a more general picture of the emergent dynamics of the school. Our model provides insight into the hydrodynamic interactions at short intra-school distances as well as the role of drag coefficient of the foil.

The model focuses on the interaction forces that arise in a reduced system of two in-line pitching foils (figure S2, and movie S2). Simulations of the two-pitching foil system (figure 5) motivate the non-dimensional expression  $f^{*2} e^{-f^* D^*} (1 + \sin(2\pi f^* D^*))$  for describing the force of the leader on the follower. The sinusoidal term describes the wake–foil interference (the Knoller–Betz effect [32] manifested as leading-edge suction) as a function of the spatial phase shift,  $f^* D^*$ , and the additive constant ( $= 1$ ) ensures the observed constructive nature of such interference. The strength of the wave-like jet is modeled with  $f^{*2}$  which is compatible with how the thrust force of an isolated pitching foil scales with  $f^*$  (figure S3), and finally,  $e^{-f^* D^*}$  captures the exponential decay in the interaction due to the dissipation of the vortical flows

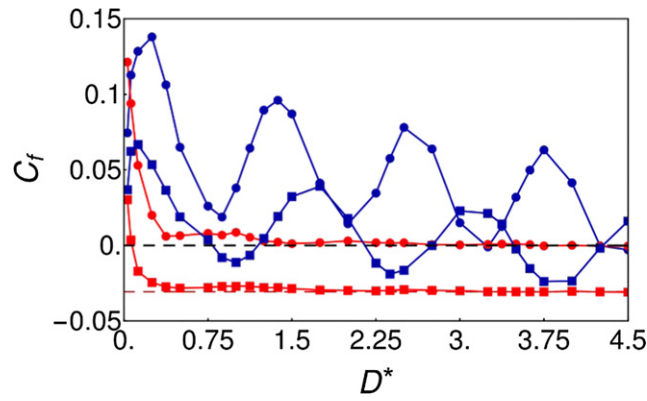


**Figure 5.** Computed time-averaged net forward force coefficient,  $C_f$ , for the leader when  $f^* = 0.88$  (●) and when  $f^* = 0.7$  (■), and for the follower when  $f^* = 0.88$  (●) and when  $f^* = 0.7$  (■) in a system of two-pitching foils in tandem as leader-follower at  $Re = 3000$ . The dashed lines correspond to the values for the isolated foil for when  $f^* = 0.88$  (— —) and for when  $f^* = 0.7$  (— —). Wake-foil interference, which is manifested as leading-edge suction, causes the net force on the follower to assume an oscillatory pattern. The blockage of the undulatory wake by the follower's leading edge increases the pressure on the leader's trailing-edge, and therefore causes a spike in the net force on the leader when the separation distance is short.

with distance (relative to the undulation wavelength of the wake). The interaction forcing of the follower on the leader is found to be inversely correlated with the distance while directly related to the strength of the wave-like jet and so is modeled as  $f^{*2}/D^*$ . In an infinite school, each foil is influenced by all its leaders and followers, but the main dynamics can be surmised by focusing only on the immediate leader and follower. The equation describing the emergent dynamics of the school at the limit of vanishing net force (i.e. cruise) is then:

$$(\alpha f^{*2} - C_d) + \beta f^{*2} e^{-f^* D^*} (1 + \sin(2\pi f^* D^*)) + \gamma \frac{f^{*2}}{D^*} = 0. \quad (3)$$

The term  $\alpha f^{*2} - C_d$  indicates the net force in the absence of interaction (i.e. an isolated pitching foil, figure S3) with  $C_d = 3.78 Re^{-0.25}$  (figure S4).  $\beta$  and  $\gamma$  are interaction strengths and are tuned by finding the best fit to our numerical data.

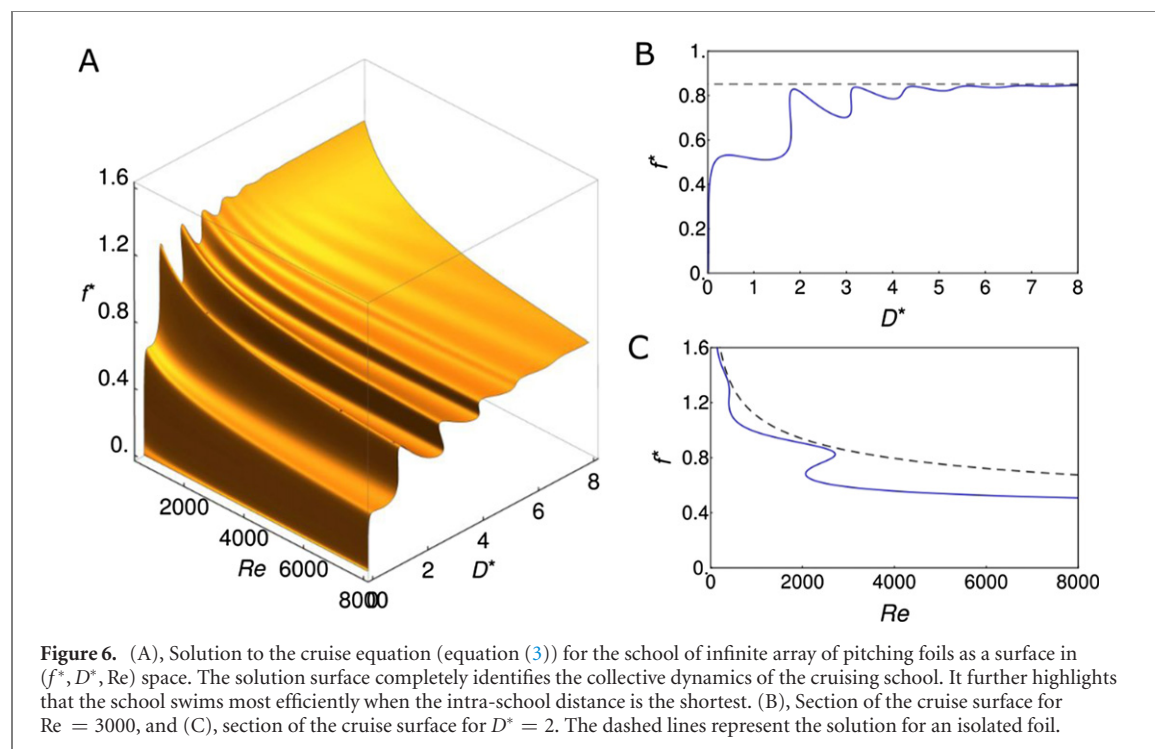
The numerical solution to equation (3) displays the complete characterization of the collective dynamics of the cruising school in three-dimensional ( $f^*, D^*, Re$ ) parameter space (figure 6(A)). For intermediate to high intra-school distances, the solution surface displays three-dimensional folds that are formed mainly due to the spatially periodic nature of the leading-edge suction. The three-dimensional folds underlie the jumps observed in the computational results of figures 3(A) and (C) as shown in figures 6(B) and (C). The values for the isolated foil are further given for comparison. For small intra-school distances, the added mass-based forcing ( $1/D^*$  term in equation (3)) dominates the interaction and the folds in the solution become subdominant, hinting that the system is strongly coupled. It is in this regime where the school swims most efficiently (i.e.  $f^*$  approaches zero). This particular regime of the cruise

solution surface is unique to foils that are capable of pitching. A school of purely heaving foils with identical motions approximates an infinitely-long heaving foil at short intra-school distances and so will completely miss this segment of the solution surface, which in our opinion is the most relevant part for engineering biomimetic swimmers.

Finally, the role of drag coefficient,  $C_d$ , is evident in the dynamics of the cruising school described by equation (3). At slow cruise speeds (low Reynolds numbers), drag coefficient is high and so is  $f^*$  given that  $f^* \sim \sqrt{C_d}$  for a cruising pitching foil [26]. As a result, the hydrodynamic interactions within the school decay faster and the solution approaches that of the isolated swimmer in shorter intra-school distances when the swimming speed is low. Our mathematical model therefore captures the main hydrodynamic characteristics obtained from the computation of the infinite school (figures 3(A) and (C)) and provides physical explanations for some of the observed schooling behaviors [5].

### 3.4. Experiments using a purpose-built robot

The interaction terms in equation (3) suggest that for a system of two pitching foils in tandem, the system can recapture some of the energy left in the oscillatory wake even when the follower does not pitch or move in an oscillatory mode. This motivated a propulsor design consisting of a stationary foil positioned in-line behind a pitching foil [figures S5(A)–(C), and movie S3]. Simulations of this system [figures S5(D) and (E)] revealed that wake-foil interaction increased the thrust on the leader relative to its hydrodynamic input power while at the same time caused the stationary follower to *also* experience thrust. Similar to the school, the leader gains extra thrust through the increase in effective added-mass on its trailing edge, while the stationary follower gains thrust through the leading-edge suction imparted by the undulatory jet



of the pitching foil (Knoller–Betz mechanism [32]). Our results indicate that this system generates thrust quite more efficiently compared to an isolated pitching foil [figure S5(E)]. Similarly inspired propulsors can be used in flapping-based biomimetic underwater vehicles to improve swimming performance.

We have developed a self-propelled autonomous fish robot capable of on-board power measurement with a propulsor resembling the system studied (figures 7(C)–(E)). In our design, a rigid foil is placed behind the flexible flapping tail and is attached to the main body using a thin rigid ring. Three cases are studied: one with the foil placed immediately behind the tail, one where the foil is distanced away from the tail by approximately 50% of the tail-chord length, and one without any foil attached. The robot without the attached foil has been designed and utilized extensively to study fish locomotion [23–25].

Comprehensive testing of the robot's swimming performance reveals that the new propulsor improves on the self-propelled speed (and cost of transport,  $P/U$ ) for a wide range of tail-beat frequencies compared to the case without a foil, when the foil is placed immediately behind the tail (figures 7(A) and (B)). In the best-case scenario (the case with  $f = 0.75$  Hz), we observe 56% improvement in speed for the same mechanical input power (equivalent to a decrease of 56% in cost of transport). For the case where the airfoil is distanced from the tail by 50% of the tail-chord length, the performance deteriorates for the most part. This ensures that the advantage gained in the former case is due to hydrodynamics and not related to the suppression of the recoil motion due to the additional surface area the robot carries. Particle image velocimetry of the flow (figures 7(F)–(H),

and movie S4–S6) shows regions of accelerated flow around the leading edge of the foil pointing to surface suction in those regions. We note that the aim here was not to optimize the design of the robot for all the swimming modes, but rather to provide a proof of concept to demonstrate the possibility of energy harvesting of such interaction-based propulsors.

To summarize, our results demonstrate how an infinite linear array of self-propelled pitching foils can save up to 70% power when swimming in a compact in-line arrangement. Compared to current studies of ideal schools, the model presented here allows for the investigation of the full parameter space by retaining the intra-school distance and Reynolds number as additional independent variables. One outcome of our results is an understanding of some of the mechanisms underlying how fish may gain hydrodynamic benefits when swimming in tandem. Our hypothesis is centered on two sources of propulsive thrust when fish swim in tandem: suction on the snout of the follower and added-mass push on the tail of the leader. The main element leading to these benefits for both the leader and the follower is the existence of, and interaction with, the oncoming undulatory flow. The elementary nature of the physics uncovered here allows fish to have a broad range of body movements while still benefiting from in-line swimming. Current observations indeed hint at fish taking advantage of such mechanisms in school [5]. We further demonstrated that these hydrodynamic improvements are present in a two-foil system even when the follower remains stationary. Building on these proposed mechanisms, we designed and tested a foil propulsor that lowered the total cost of locomotion of a biomimetic underwater robot by up to 56%. This



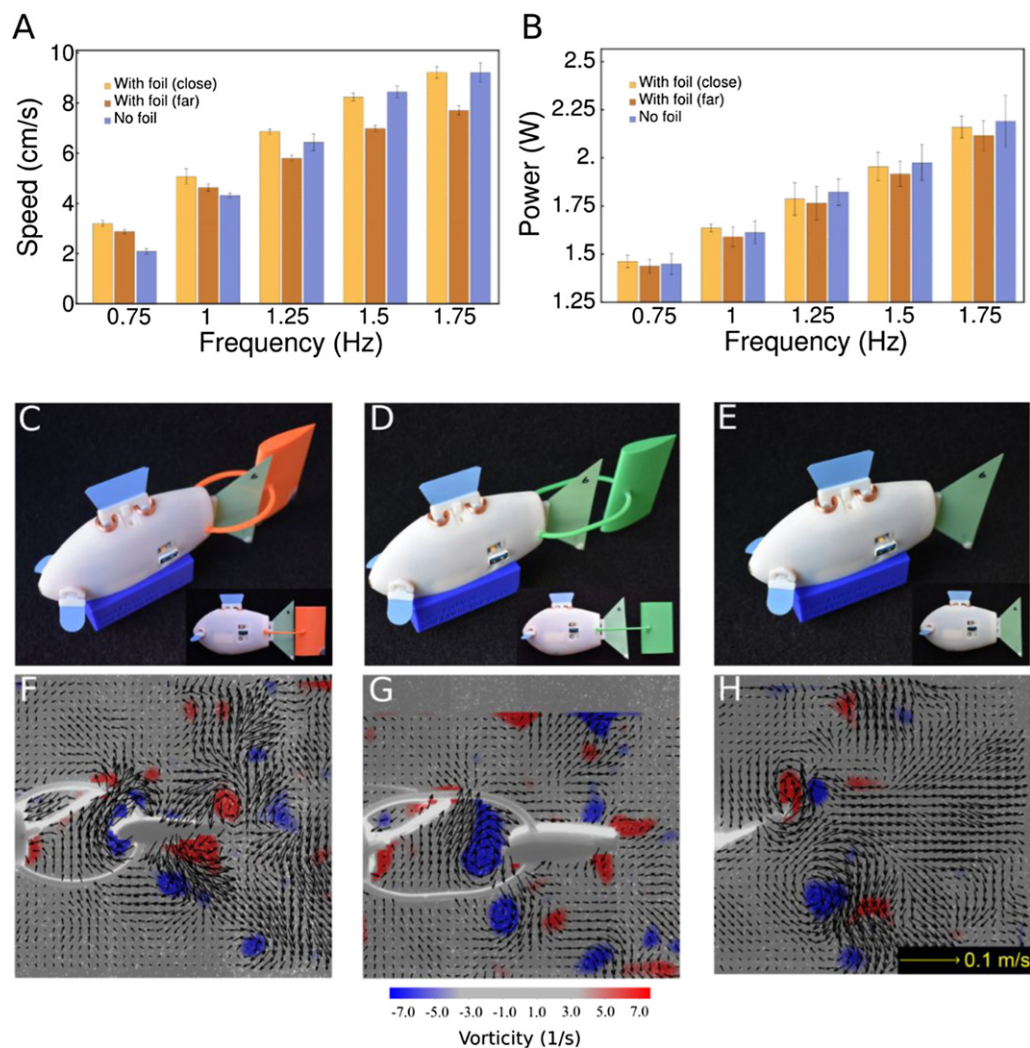


**Figure 7.** Informed by the underlying principles of energy benefits of the school, we designed and tested novel interaction-based propulsors attached to a self-propelled underwater fish robot. (A) and (B) Measured swimming speed and corresponding electrical power as a function of the tail-beat frequency for the case (C), with the foil placed immediately behind the tail, and (D), the case where the foil is spaced away from the tail by 50% of the tail-chord length, and (E), the case without the foil. Standard deviations in measured speed and power are given as bar lengths for each case with  $N = 5$  independent experiments. (F)–(H), flow visualization using particle image velocimetry shows vorticity contours superimposed on their corresponding velocity vectors for all three cases at cruise when the flapping frequency is at 0.75 Hz.

demonstration serves as an example of how these new findings can be utilized to save energy in engineered systems.

### Competing interests

Authors declare no competing interests.

### Authors contributions

MS, HH, AS, and GVL developed the concept and designed the study. MS performed the simulations and analyzed the resulting data. MS, HH, and AS developed the mathematical model. FB and RN designed and manufactured the robot. MS and FB performed the experiments and analyzed the resulting data. All authors contributed to writing the paper.

### Acknowledgments

GVL acknowledges funding by the Office of Naval Research (Tom McKenna, Program Manager, ONR 341), Grant No. N00014-15-1-2234, and by ONR MURI Grant No. N000141612515 monitored by R Brizzolara. FB and RN received additional support from the Wyss Institute for Biologically Inspired Engineering.

### ORCID iDs

Mehdi Saadat <https://orcid.org/0000-0002-3068-2538>

Florian Berlinger <https://orcid.org/0000-0002-9778-722X>

George V Lauder <https://orcid.org/0000-0003-0731-286X>

## References

- [1] Shaw E 1962 The schooling of fishes *Sci. Am.* **206** 128–41
- [2] Cushing D H and Jones F R H 1968 Why do fish school? *Nature* **218** 918–20
- [3] Weihs D 1973 Hydromechanics of fish schooling *Nature* **241** 290–1
- [4] Breder C M 1965 Vortices and fish schools *Zoologica* **50** 97–114
- [5] Marras S, Killen S S, Lindström J, McKenzie D J, Steffensen J F and Domenici P 2015 Fish swimming in schools save energy regardless of their spatial position *Behav. Ecol. Sociobiol.* **69** 219–26
- [6] Partridge B L and Pitcher T J 1979 Evidence against a hydrodynamic function for fish schools *Nature* **279** 418–9
- [7] Pitcher T J and Partridge B L 1979 Fish school density and volume *Mar. Biol.* **54** 383–94
- [8] Partridge B L, Pitcher T, Cullen J M and Wilson J 1980 The three-dimensional structure of fish schools *Behav. Ecol. Sociobiol.* **6** 277–88
- [9] Hemelrijk C, Reid D, Hildenbrandt H and Padding J 2015 The increased efficiency of fish swimming in a school *Fish Fisheries* **16** 511–21
- [10] Zhu X, He G and Zhang X 2014 Flow-mediated interactions between two self-propelled flapping filaments in tandem configuration *Phys. Rev. Lett.* **113** 238105
- [11] Newbolt J W, Zhang J and Ristroph L 2019 Flow interactions between uncoordinated flapping swimmers give rise to group cohesion *Proc. Natl Acad. Sci. USA* **116** 2419–24
- [12] Dai L, He G, Zhang X and Zhang X 2018 Stable formations of self-propelled fish-like swimmers induced by hydrodynamic interactions *J. R. Soc. Interface* **15** 20180490
- [13] Maertens A P, Gao A and Triantafyllou M S 2017 Optimal undulatory swimming for a single fish-like body and for a pair of interacting swimmers *J. Fluid Mech.* **813** 301–45
- [14] Ramanarivo S, Fang F, Oza A, Zhang J and Ristroph L 2016 Flow interactions lead to orderly formations of flapping wings in forward flight *Phys. Rev. Fluids* **1** 071201
- [15] Dewey P A, Boschitsch B M, Moored K W, Stone H A and Smits A J 2013 Scaling laws for the thrust production of flexible pitching panels *J. Fluid Mech.* **732** 29–46
- [16] Boschitsch B M, Dewey P A and Smits A J 2014 Propulsive performance of unsteady tandem hydrofoils in an in-line configuration *Phys. Fluids* **26** 051901
- [17] Lewin G C and Haj-Hariri H 2003 Modelling thrust generation of a two-dimensional heaving airfoil in a viscous flow *J. Fluid Mech.* **492** 339–62
- [18] Floryan D, Van Buren T and Smits A J 2018 Efficient cruising for swimming and flying animals is dictated by fluid drag *Proc. Natl Acad. Sci. USA* **115** 8116–8
- [19] Becker A D, Masoud H, Newbolt J W, Shelley M and Ristroph L 2015 Hydrodynamic schooling of flapping swimmers *Nat. Commun.* **6** 8514
- [20] ANSYS Academic Research Help System, ANSYS CFX-Solver Theory Guide (ANSYS, Inc) 2020
- [21] Menter F 1993 Zonal two equation k- $\omega$  turbulence models for aerodynamic flows *AIAA* **93** 1993–2906
- [22] Floryan D, Van Buren T, Rowley C W and Smits A J 2017 Scaling the propulsive performance of heaving and pitching foils *J. Fluid Mech.* **822** 386–97
- [23] Berlinger F, Dusek J, Gauci M and Nagpal R 2018 Robust maneuverability of a miniature, low-cost underwater robot using multiple fin actuation *IEEE Robot. Autom. Lett.* **3** 140–7
- [24] Berlinger F, Saadat M, Haj-Hariri H, Lauder G V and Nagpal R 2020 A reconfigurable, multi-fin, and autonomous biomimetic robot for fish-like swimming *Bioinspir. Biomim.* **16** 026018
- [25] Berlinger F, Gauci M and Nagpal R 2020 Implicit coordination for 3D underwater collective behaviors in a fish-inspired robot swarm *Sci. Robot.* **6** eabd8668
- [26] Saadat M, Fish F E, Domel A G, Di Santo V, Lauder G V and Haj-Hariri H 2017 On the rules for aquatic locomotion *Phys. Rev. Fluids* **2** 083102
- [27] Nath T, Mathis A, Chen A C, Patel A, Bethge M and Mathis M W 2019 Using DeepLabCut for 3D markerless pose estimation across species and behaviors *Nat. Protoc.* **14** 2152–76
- [28] Rohr J J and Fish F E 2004 Strouhal numbers and optimization of swimming by odontocete cetaceans *J. Exp. Biol.* **207** 1633–42
- [29] Bainbridge R 1958 The speed of swimming of fish as related to size and to the frequency and amplitude of the tail beat *J. Exp. Biol.* **35** 109–33
- [30] Ashraf I, Bradshaw H, Ha T-T, Halloy J, Godoy-Diana R and Thiria B 2017 Simple phalanx pattern leads to energy saving in cohesive fish schooling *Proc. Natl Acad. Sci. USA* **114** 9599–604
- [31] Fish F E and Lauder G V 2006 Passive and active flow control by swimming fishes and mammals *Annu. Rev. Fluid Mech.* **38** 193–224
- [32] Jones K D, Dohring C M and Platzer M F 1998 Experimental and computational investigation of the Knoller–Betz effect *AIAA J.* **36** 1240–6
- [33] Buren T V, Floryan D and Smits A J 2019 Scaling and performance of simultaneously heaving and pitching foils *AIAA J.* **57** 3666–77